RSC Advances

ROYAL SOCIETY OF CHEMISTRY

www.rsc.org/advances

Curcumin-loaded, folic acid-functionalized magnetite particles for targeted drug delivery

Melessa Salem[a], Ying Xia[b], Alison Allan[b], Sohrab Rohani[a,c] and Elizabeth R. Gillies[a,c,d*]

[a]Biomedical Engineering Graduate Program, The University of Western Ontario, 1151 Richmond Street, London, Ontario, Canada N6A 5B9

[b]London Regional Cancer Program, 790 Commissioners Road East, London, Ontario, N6A 4L6

[c]Department of Chemical and Biochemical Engineering, The University of Western Ontario, 1151 Richmond Street, London, Ontario, Canada N6A 5B9

[d]Department of Chemistry, The University of Western Ontario, 1151 Richmond Street, London, Ontario, Canada N6A 5B7

*Author to whom correspondence should be addressed; email: egillie@uwo.ca

Table of contents entry

Magnetite nanoparticles were coated with amine-terminated poly(propylene glycol) and β-cyclodextrin. Encapsulation of curcumin into the β-cyclodextrin and functionalization of poly(propylene glycol) with folic acid afforded a targeted curcumin delivery system.

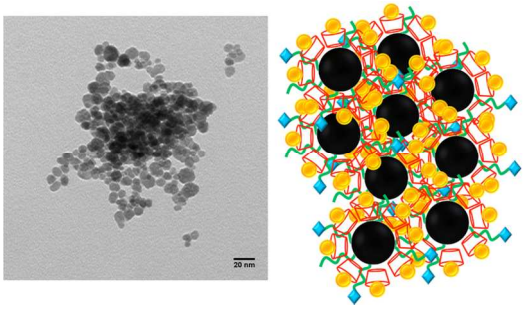

Abstract

Precipitation of Fe_3O_4 from $FeSO_4$ in the presence of NH_4OH, amine-terminated poly(propylene glycol) (PPG-NH_2) and β-cyclodextrin (β-CD) afforded magnetite particles coated with PPG-NH_2 and β-CD. The sizes of the particles, as characterized by dynamic light scattering and electron microscopy, depended on the preparation conditions, but the essential magnetite structure and magnetic properties were retained in the presence of the surface coating. The terminal amine of PPG-NH_2 was used for the conjugation of folic acid (FA), with the aim of targeting cancer cells overexpressing the FA receptor. Curcumin, a promising chemotherapeutic exhibiting low aqueous solubility and rapid metabolic degradation was encapsulated into the β-CD cavity to enhance its delivery to cancer cells. The loading of curcumin and its release rate was found to depend on the particle size and composition, with sustained curcumin release observed for some systems. The uptake of the particles into MDA-MB-231 and MDA-MB-468 human breast cancer cells were compared and the toxicities of the curcumin-loaded particles were compared to the free drug and to particles without curcumin.

Introduction

The development of new particle-based materials for the delivery of therapeutics is a promising approach for improving the dispersibility, stability, and biodistribution behavior of new drug candidates.[1-3] In addition, the selective delivery of drugs to their target sites *in vivo* can result in enhanced therapeutic efficacy and decreased systemic toxicity. This is particularly relevant for anti-cancer therapeutics, which frequently result in adverse effects including nausea, liver damage, cardiotoxicity, and

immunosuppression.[4,5] In this context, there have been numerous delivery systems developed for chemotherapeutics. These have included dendrimers,[6,7] micelles,[8,9] liposomes,[10] polymersomes,[11] and lipid[2] or polymer-based[3,12] solid particles. These materials can be passively targeted to tumor tissue through the enhanced permeation and retention effect or actively targeted using ligands such as small molecules, peptides, or antibodies.[13-15] Systems including a liposomal formulation of doxorubicin[16] and an albumin-based formulation of paclitaxel have been translated to the clinic for the treatment of several cancers.[17]

Of the wide range of materials that are available for the preparation of drug delivery systems, magnetite (iron oxide, Fe_3O_4) nanoparticles are of particular interest due to their small size, low toxicity, high stability and surface area, and their magnetic properties.[18-20] As they can be tailored in terms of their size, morphology, and surface chemistry, they have been investigated for many applications. In magnetic resonance imaging, they have been extensively used in both cellular and molecular imaging.[21,22] They are also under investigation for their application in hyperthermia treatment of cancer as they can provide high localized heating in the presence of an alternating magnetic field.[23,24] Their ability to provide high MRI contrast and hyperthermia effects has also inspired significant recent interest in their application as drug delivery systems, where they can provide theranostic and dual therapeutic properties.[25,26] Furthermore, magnetite particles can be magnetically targeted to specific locations *in vivo*, providing an additional function to enhance the therapeutic efficacy of loaded drugs.[18,20]

Curcumin is a natural polyphenol derived from *Curcumo longa*, a plant from the ginger family, and is the principle component of the dietary spice turmeric. While used

for centuries in Asia to treat a diverse array of illnesses ranging from infections to respiratory complications, it has recently garnered significant interest in Western medicine for its anti-inflammatory, antioxidant, chemopreventive, and chemotherapeutic properties.[27,28] Curcumin's anti-cancer properties are proposed to arise from its ability to interfere with several biochemical pathways involved in the proliferation of cancer cells.[29,30] However, its translation to the clinic has been greatly hindered by its poor solubility, chemical instability, and rapid metabolism *in vivo*.[31,32] To address this, various approaches have been explored to enhance the bioavailability of curcumin and to deliver it effectively to cancer cells. For example, curcumin has been co-crystallized with compounds such as resorcinol, pyrogallol, ferulic acid, and L-tartaric acid to enhance its dissolution rate,[32,33] and it has been encapsulated into liposomes,[34,35] exosomes,[36] micelles,[37-39] and particles.[40-42] It has also been incorporated onto the surface of magnetite nanoparticles coated with β-cyclodextrin (β-CD) and amphiphilic pluronic polymers and the resulting system was shown to provide enhanced toxicity to breast, pancreatic, ovarian, and prostate cancer cell lines *in vitro*.[43-45]

With the aim of developing a multifunctional magnetite system capable of targeted curcumin delivery, we describe here the preparation and characterization of magnetite particles coated with β-CD and amine-terminated poly(propylene glycol) (PPG-NH_2) (Figure 1). Curcumin encapsulation into the β-CD cavity has been demonstrated.[43,44,46,47] In addition, PPG has been well-established to form complexes with β-CD, with the polymer chain weaving through the β-CD cavity.[48,49] The terminal amine is used to conjugate folic acid (FA), a ligand that has been demonstrated to target the FA receptor, which is overexpressed on the cell surface of some cancer cells.[50,51] The abilities

of the particles to encapsulate curcumin and release it in a sustained manner is studied. In addition, the effects of both folate-functionalized and control particles on MDA-MB-231 and MDA-MB-468 human breast cancer cells is studied *in vitro*. To the best of our knowledge this is the first ligand-targeted curcumin-magnetite delivery system and the first detailed study of the effect of particle composition on curcumin encapsulation and release. The targeting afforded by folic acid, combined with the potential to perform magnetic targeting, is expected to afford the selective delivery of curcumin to cancer cells.

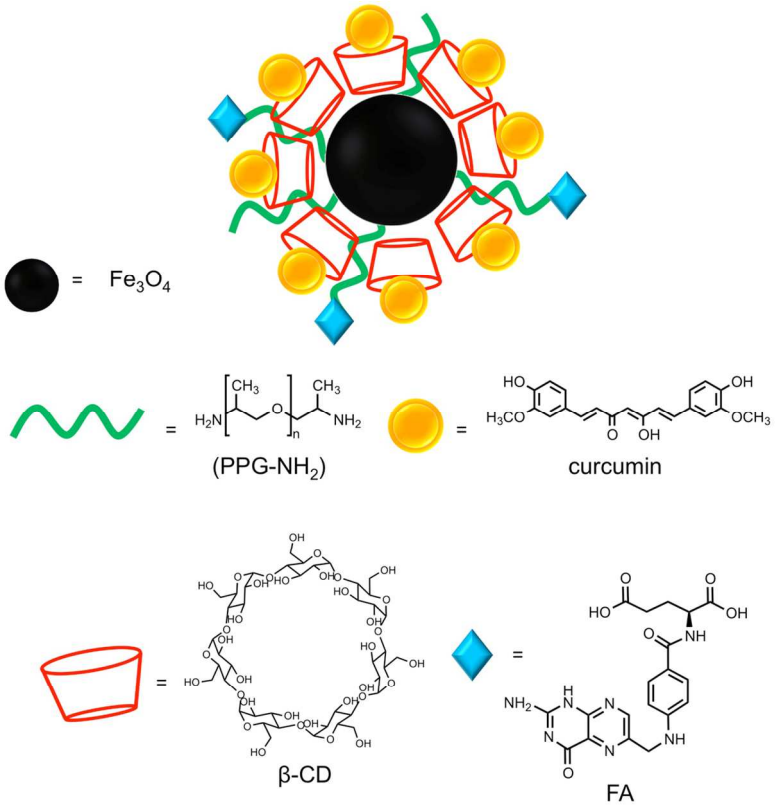

Figure 1. Schematic of a FA-conjugated curcumin-loaded magnetite nanoparticle.

Results and Discussion

Particle preparation and characterization

Common methods for the synthesis of magnetite nanoparticles include precipitation, thermal decomposition, and hydrothermal/solvothermal synthesis.[52-54] In the current work, a precipitation method based on only Fe^{2+} was used. Unlike the traditional coprecipitation method where Fe^{2+} and Fe^{3+} salts must be used in a precise 1:2 molar ratio in order to avoid the formation of γ-Fe_2O_3,[52,55] this method involves an *in situ* oxidation of Fe^{2+} to Fe^{3+} by molecular oxygen to form Fe_3O_4.[56] As shown in Scheme 1, particles were prepared by the addition of β-CD to a solution of $FeSO_4$ and PPG-NH_2 under alkaline conditions. X-ray diffraction analysis was used to confirm that the resulting particles were magnetite (ESI, Figure S1). As shown in Table 1, different ratios of β-CD, PPG-NH_2, and $FeSO_4$ were used to prepare particles **P1** – **P4** with the aim of exploring the effects of these ratios on the particle properties. For example, it was expected that the concentration of PPG-NH_2 and its ratio to β-CD would impact the particle size as this polymer can act as a stabilizer by adsorbing on the nanoparticle surface.[57]

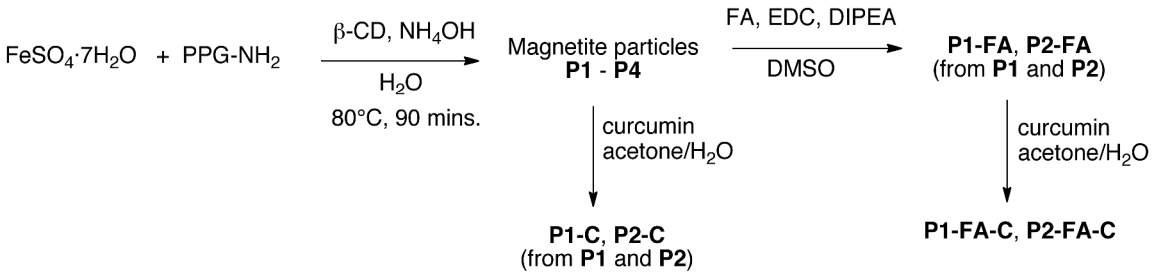

Scheme 1. Particle synthesis and curcumin loading.

Table 1. Particle preparation conditions as well as folic acid and curcumin content of the synthesized particles.

Particle	mmol PPG-NH_2 : mmol β-CD ($FeSO_4 \cdot 7H_2O$ is constant at 5 mmol in 70 mL of H_2O total)	Folic Acid	Curcumin
Control	-	-	-
P1	0.25 : 1.0	-	-
P2	0.50 : 1.0	-	-
P3	1.0 :1.0	-	-
P4	1.0 :0.5	-	-
P1-C	0.25 : 1.0	-	+
P2-C	0.50 : 1.0	-	+
P1-FA	0.25 : 1.0	+	-
P2-FA	0.50 : 1.0	+	-
P1-FA-C	0.25 : 1.0	+	+
P2-FA-C	0.50 : 1.0	+	+

The sizes of the resulting particles were measured by dynamic light scattering (DLS) and transmission electron microscopy (TEM). As shown in Table 2, DLS measurements performed at high concentration indicated that particles with Z-average diameters ranging from 220 to 1000 nm existed in the equilibrium state. However, TEM (Figure 2a and Figures S7 - S9) as well as DLS measurements performed on diluted and sonicated samples confirmed that these were reversible aggregates of spherical

nanoparticles with diameters of ~10 nm. There were no significant trends in the aggregate diameter with respect to the ratio of PPG-NH_2:β-CD in **P1** – **P4**. However, the results suggest that sufficiently high concentrations of both PPG-NH_2 and β-CD were required for the formation of the smaller aggregates in **P2** and **P3** and that the presence of more β-CD than PPG-NH_2 in the case of **P2** resulted in the smallest aggregates. This may be attributed to the increased hydrophilicity of β-CD relative to PPG-NH_2, which would result in higher particle dispersibility in water. TEM imaging of control particles prepared in the absence of PPG-NH_2 and β-CD revealed much larger aggregates that were impossible to measure by DLS (Figure 2b). In general, the sizes of the nanoparticle aggregates would be most suitable for localized or pulmonary drug delivery where the aggregated state of the magnetite would lead to enhanced magnetic properties.[58] Intravascular delivery would likely result in significant uptake by the reticuloendothelial system.[59] However, recent work by Martens and coworkers has shown that through a combination of Lorentz forces and the hydrodynamic forces associated with turbulent flow, it was possible to deaggregate nanoparticles using a 0.31 T magnetic field.[60] This would be a potential approach to deaggregate the particles in magnetically targeted delivery.

Table 2. Aggregate and individual nanoparticle sizes as measured by DLS. Errors on the measurements correspond to the standard deviation of three measurements.

Sample	**P1**	**P2**	**P3**	**P4**
Z-average aggregate diameter (nm)	1000 ± 75	220 ± 10	355 ± 5	443 ± 9
Polydispersity index	0.35 ± 0.09	0.30 ± 0.06	0.43 ± 0.02	0.31 ± 0.06
Z-average diameter of individual particles (nm)	13 ± 5.6	10 ± 6	11 ± 7	9.1 ± 3.4
Polydispersity index	0.20 ± 0.1	0.24 ± 0.07	0.27 ± 0.1	0.28 ± 0.07

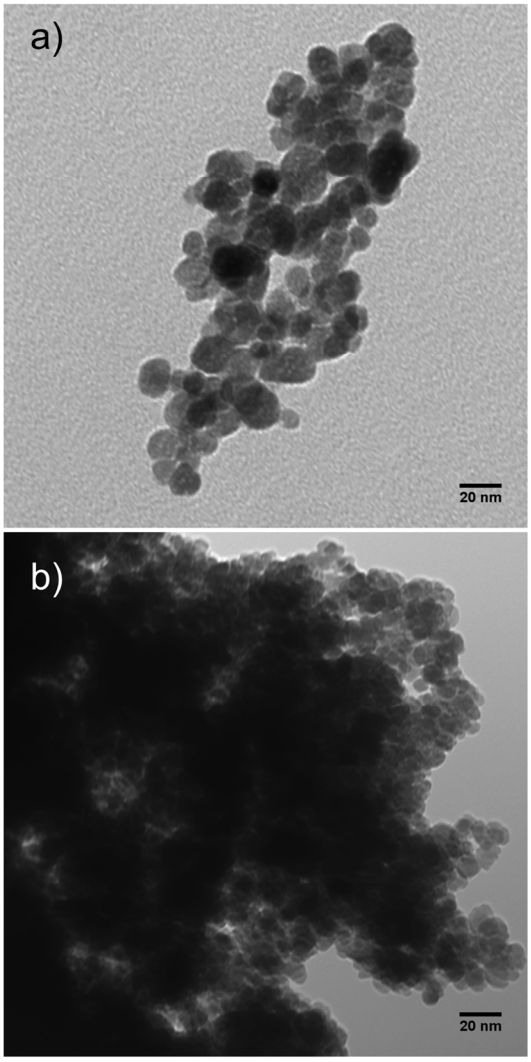

Figure 2. TEM images of a) particles P2 and b) uncoated control particles.

In order to study both large and small aggregates, **P1** and **P2** were used in further experiments. The magnetic properties of uncoated control particles, and **P2** were studied to determine how the magnetic properties were affected by the presence of surface coatings. Bulk magnetite is ferrimagnetic at room temperature due to the presence of at least two sublattices composed of the two different cationic sites in the structure (tetrahedral site of Fe^{3+} and octahedral site of both Fe^{3+} and Fe^{2+}).[61] However, magnetite in the form of nanoparticles (≤ ~20 nm) exhibits superparamagnetic behavior[61,62] as a

result of easy magnetization along the crystallographic axis [111].[61] As shown in Figure 3, this behavior is evident in the control and **P2** based on the low coercivity of each sample, which is characteristic of a superparamagnetic material.[61,63] Surface modification with β-CD and PPG-NH_2 in **P2** modestly decreased the saturation magnetization (M_s), remnant magnetization (M_r) and coercivity, but the particles still retained superparamagnetic properties.

a)

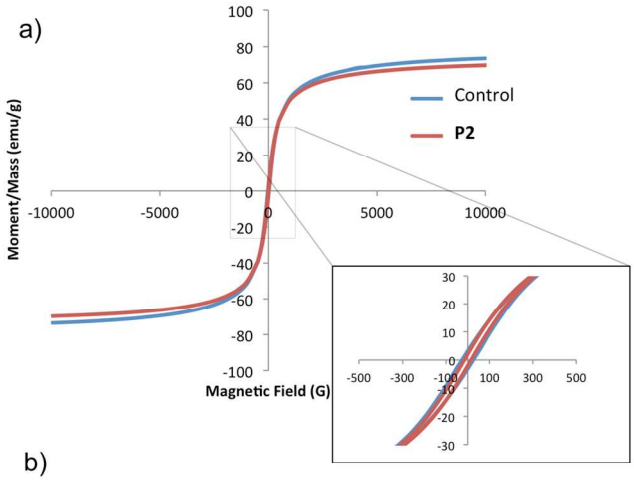

b)

Sample	Saturation Magnetization (M_s) (emu/g)	Remnant Magnetization (M_r) (emu/g)	Coercivity (G)
Uncoated control	73.6	3.1	26.0
P2	69.8	2.0	15.4

Figure 3. a) Magnetization curves of control uncoated particles and **P2**; b) Magnetic properties of the particles obtained from the curves in a).

Because nuclear magnetic resonance spectroscopy could not be used to verify the presence and chemical structures of the particles coatings, Fourier transform infrared

(FTIR) spectroscopy was used to confirm the presence of characteristic functional groups in the samples. As shown in Figure 4a, the spectrum of the control uncoated particles had peaks at approximately 3450 $cm^{-1}$and 1630 cm^{-1} corresponding to stretching and bending modes of residual water on the particles.[64] The spectra of pure β-CD and PPG-NH_2 are shown in Figures 4b and c respectively. β-CD undergoes C-H stretching at 2900 cm^{-1} and O-H stretching and bending at 3400 cm^{-1} (broad) and 1630 cm^{-1} respectively. The spectrum of PPG-NH_2 is characterized by strong C-H stretching peaks between 2800 cm^{-1} and 3000 cm^{-1}. The spectrum of the coated particles (**P2**) exhibits the features of both β-CD and PPG-NH_2, confirming the presence of both of these molecules on the particle surface (Figure 4d).

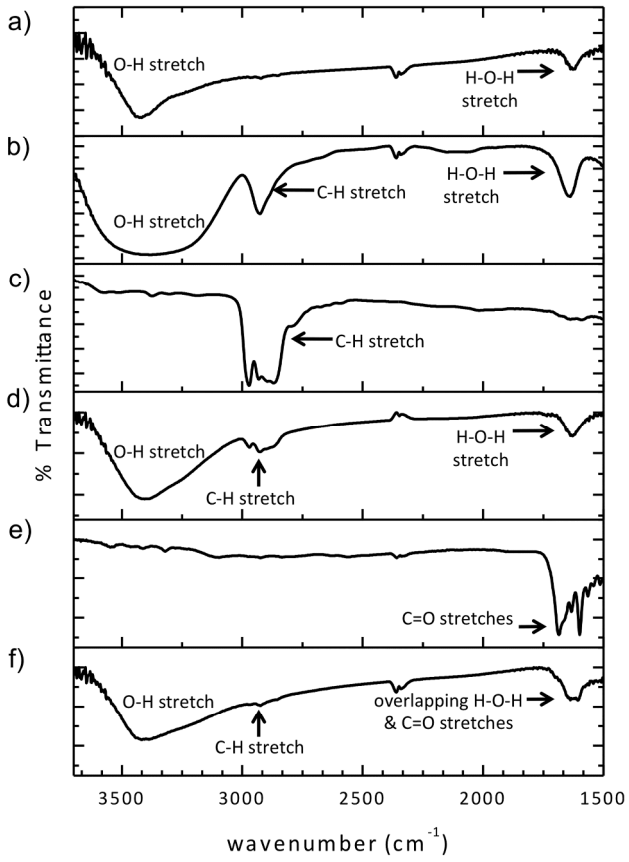

Figure 4. FTIR spectra of a) control uncoated particles, b) β-CD, c) PPG-NH2, d) **P2**, e) FA, and f) sample **P2-FA**.

Conjugation of folic acid to P1 and P2

As shown in Scheme 1, folic acid (FA) was conjugated to the amine termini of PPG-NH_2 in dimethylsulfoxide (DMSO) by reaction with *N*-(3-dimethylaminopropyl)-*N*′-ethylcarbodiimide (EDC) in the presence of *N,N*-diisopropylethylamine (DIPEA) first at ambient temperature for 3 hours, then at 35 °C for 2 days. This reaction was performed on **P1** and **P2**. After isolation through sedimentation, the resulting particles were extensively washed with ethanol and then dried to provide **P1-FA** and **P2-FA**. The concentration of FA in the washings was quantified by UV-visible spectroscopy. This allowed the percentage of conjugated FA relative to the amount added, to be calculated according to equation (1):

$$\%\ Conjugation = \frac{w_i - w_s}{w_i} \times 100\% \qquad (1)$$

where, w_i is the weight of folic acid used in the coupling reaction, and w_s is the weight of folic acid remaining in the supernatant.

The analysis suggested that 27 ± 9% and 23 ± 6% of FA used in the reaction was conjugated to **P1-FA** and **P2-FA** respectively, providing approximately 0.5 μmol of FA per mg of **P1-FA** and 0.4 μmol of FA per mg of **P2-FA**. Despite **P2** having more PPG-NH_2 in the initial synthesis, the FA loadings of **P1-FA** and **P2-FA** were not different statistically. The resulting particles were also characterized by FTIR spectroscopy. The spectrum of free FA is shown in Figure 4e. Characteristic peaks corresponding to the amide and carboxylic acid C=O stretching modes were observed, and these were also

observed in the spectrum of **P2-FA** (Figure 4f), suggesting the presence of FA in this system. While characterization of the coupling on the particles by ^{1}H NMR spectroscopy was not possible due to the magnetic properties of the particles, a model reaction was performed on PPG-NH_2 under the same conditions. Characterization of the product by ^{1}H NMR spectroscopy demonstrated that the coupling had proceeded in good yield, providing further evidence for the successful reaction (Figure S11). No change in the XRD pattern was observed following FA conjugation, confirming that this reaction did not affect the magnetite structure (Figure S1).

Curcumin loading and *in vitro* release

It has been well established that curcumin can form an inclusion complex with cyclodextrin.[43,44,46,47] To accomplish this with the magnetite particles **P1** and **P2**, a solvent exchange method was used, involving the addition of an acetone solution of curcumin to an aqueous suspension of the particles, following by acetone evaporation to provide **P1-C** and **P2-C**. After washing, the amount of encapsulated curcumin was measured by extraction of the curcumin into ethanol and quantification by UV-visible spectroscopy. In order to optimize the loading of curcumin, it was added in varying ratios to **P1** and **P2** and the corresponding encapsulation efficiencies were calculated. As shown in Figure 5, the encapsulation efficiencies increased up to 0.3 mg of curcumin/mg of particles, then decreased at the highest curcumin ratio of 0.5 mg of curcumin/mg of particles. This suggests that the cyclodextrin cavities were saturated somewhere between 0.3 and 0.5 mg of curcumin/mg of particles. Based on these results, 0.3 mg of curcumin/mg of particles was selected for future experiments. At this loading ratio,

encapsulation efficiencies of 73 ± 4% and 86 ± 5% were obtained for **P1-C** and **P2-C**, corresponding to drug loading contents of 23 ± 1 wt% and 26 ± 2 wt%. When samples containing FA (**P1-FA** and **P2-FA**) were loaded at 0.3 mg of curcumin/mg of particles, considerably lower encapsulation efficiencies of 41 ± 4% and 31 ± 2% were obtained, corresponding to drug loading contents of 12 ± 1wt% and 9.0 ± 0.40 wt%, respectively. This significant decrease in drug loading can be attributed to the presence of the FA, which may prevent access of curcumin to the β-CD cavity by residing either near or inside the cavities.

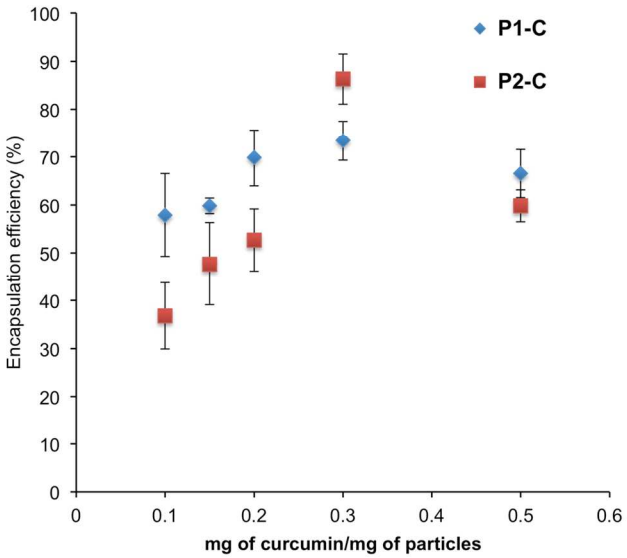

Figure 5. Encapsulation efficiency as a function of curcumin/particle weight ratio during the loading procedure.

The release of curcumin from the particles was first studied at 37 °C in pH 7.4 phosphate buffered saline containing 0.10% Tween 80. At each time point, the particles were magnetically separated from the release medium. The concentration of curcumin in

the release medium was measured using UV-visible spectroscopy, and the particles were immersed in fresh release medium. As shown in Figure 6a and b, both **P1-C** and **P1-FA-C** exhibited a significant burst release of ~80% of the curcumin during the first 8 hours. **P1** were the particles existing as larger micrometer sized aggregates and this result suggests that a large fraction of the "encapsulated" curcumin may have actually been bound to the surface of these aggregates or in between individual particles within the aggregate rather than specifically within the β-CD cavity. To investigate whether this release profile actually reflected the simple dissolution of curcumin during the experiment, the dissolution of the same quantity of solid free curcumin was measured using the same procedure. As shown in Figure S12 (ESI), this free curcumin dissolved over a period of 5 hours. This dissolution rate is very similar to the observed release profile of curcumin from **P1**, confirming that in this system the β-CD did not afford prolonged drug release.

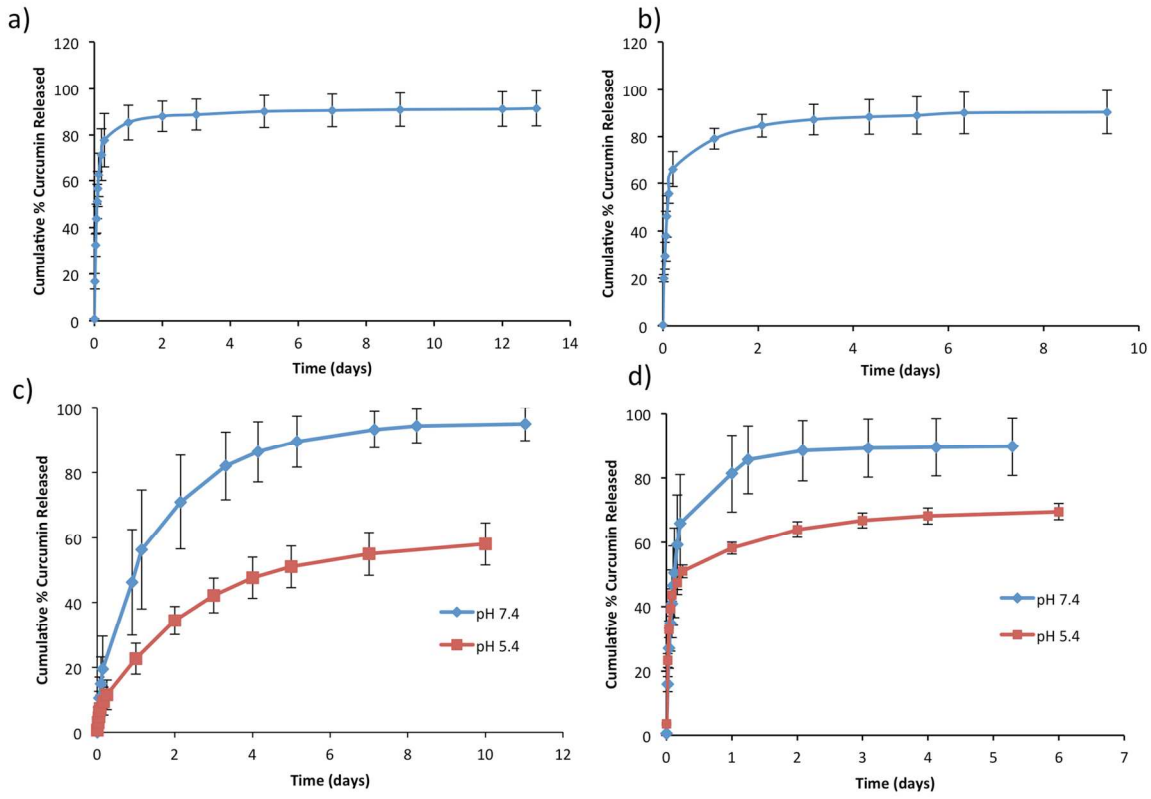

Figure 6. *In vitro* curcumin release profiles for a) **P1-C**, b) **P1-FA-C**, c) **P2-C**, and d) **P2-FA-C**.

On the other hand, **P2-C** exhibited minimal burst release and the release of curcumin occurred over a period of 5-10 days (Figure 6c). **P2-FA-C** (Figure 6d) exhibited more burst release than **P2-C** but less than the **P1** samples and released curcumin over a period of 2-3 days. This suggests that the presence of FA may have resulted in a portion of the curcumin being more loosely bound, though the reasons for this are not obvious. To mimic the mildly acidic conditions occurring in tumor tissue and in the lysosomes of cells, the release of curcumin from **P2** and **P2-FA** was also studied in 0.2 M, pH 5.4 acetate buffer. As shown in Figures 6c and d, the release was somewhat slower at acidic pH. This behavior can be attributed to the vinylogous carboxylic acid moiety present in curcumin. At mildly acidic pH, this group would be less ionized,

resulting in increased hydrophobicity and increased tendency to remain encapsulated in the β-CD cavity.

***In vitro* studies**

Based on their more sustained curcumin release profiles, **P2-C** and **P2-FA-C** were selected for *in vitro* studies. The human breast cancer cell lines MDA-MB-231 and MDA-MB-468 were chosen, as they are well-studied and clinically relevant cell lines. These cell lines have been used in other work involving FA targeting.[65,66] However, these previous reports suggest contradictory information regarding the relative expression levels of the FA receptor. For this reason, our MDA-MB-231 and MDA-MB-468 FA receptor expression was evaluated using flow cytometry.

As shown in Figure 7a, the results suggested that the MDA-MB-468 cells exhibit approximately 10-fold higher FA receptor expression than the MDA-MB-231 cells. Therefore, it was expected that the MDA-MB-468 cells should exhibit higher uptake of the FA-functionalized particles. To test this, both **P2** and **P2-FA** were labeled with fluorescein isothiocyanate (FITC) and their uptake by MDA-MB-231 and MDA-MB-468 cells was evaluated by flow cytometry. As shown in Figure 7b, **P2-FA** exhibited 3.2-fold greater uptake into the MDA-MB-231 cells than **P2**. This might be attributed to some folate receptor expressed on the MDA-MB-231 cells. The MDA-MB-468 cells exhibited a higher level of particle uptake in general, but still the uptake was 3.9-fold higher for **P2-FA** than **P2**. Overall, these results suggest that FA targeting can provide higher levels of cell uptake in general in these cancer cells, which can be favorable for the delivery of curcumin. However, the higher general uptake of particles by MDA-MB-468 cells and

the modest differences in folate receptor expression between MDA-MB-231 and MDA-MB-468 cells makes it challenging to elucidate the specific contributions of these aspects to the observed high level of uptake of **P2-FA** into MDA-MB-468 cells. Fluorescence confocal microscopy was also used to visualize the cell uptake of the particles. As shown in Figure 8, the images confirm that the particles were indeed taken up by the cells and that they were distributed throughout the cytoplasm, possibly in endosomal or lysosomal compartments.

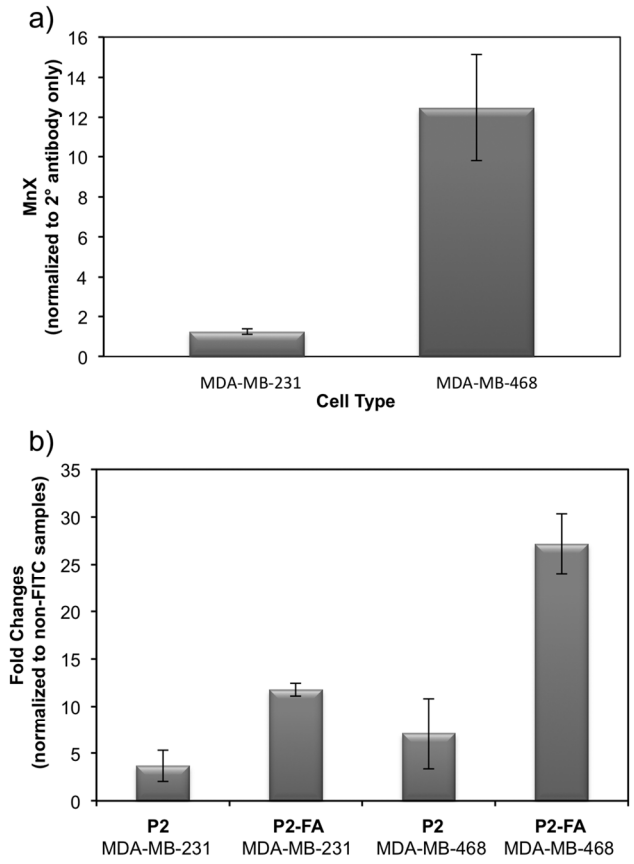

Figure 7. a) Folate receptor expression on MDA-MB-231 and MDA-MB-468 cells as measured by flow cytometry. Cell staining was performed using a mouse anti-human folate receptor antibody and an Alexa Fluor® 488-conjugated goat anti-mouse IgG; b)

Comparison of the uptake of samples **P2** and **P2-FA** by MDA-MB-231 and MDA-MB-468 cells based on flow cytometry using FITC-labeled particles.

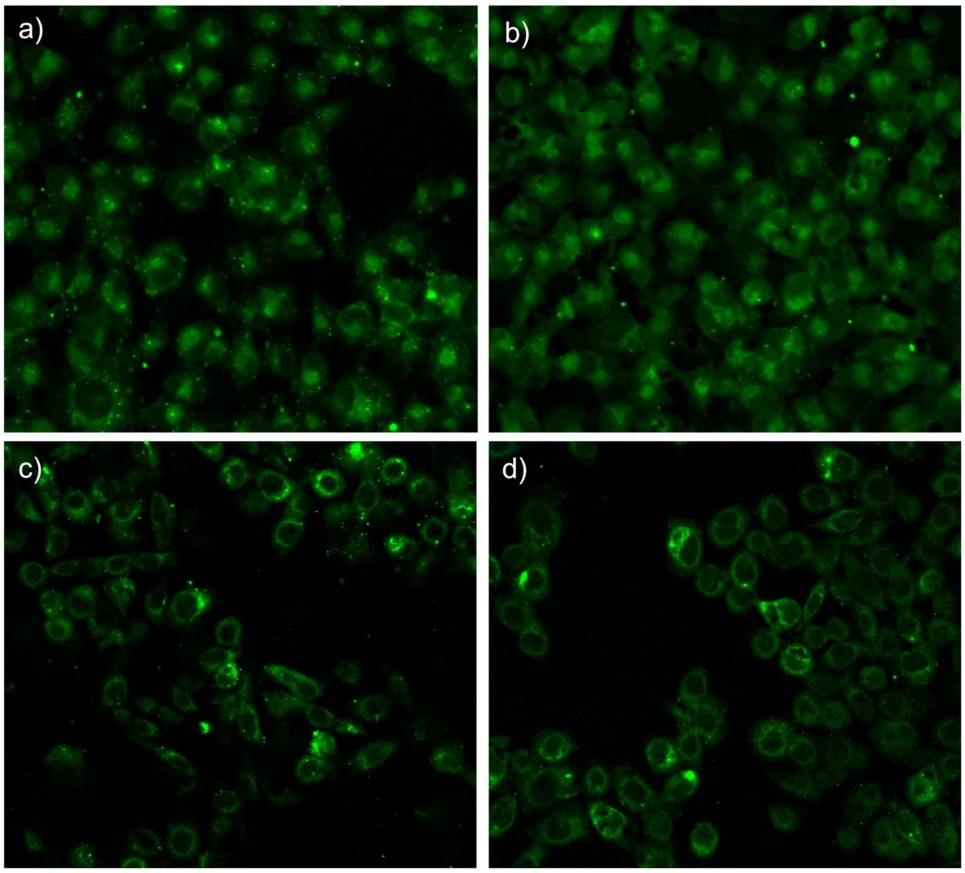

Figure 8. Fluorescence confocal microscopy images of cells following a 4 hour incubation with particles: a) **P2** in MDA-MB-231 cells; b) **P2-FA** in MDA-MB-231 cells; c) **P2** in MDA-MB-468 cells; d) **P2-FA** in MDA-MB-468 cells. The green fluorescence corresponds to the fluorescein label on the particles.

Before conducting cytotoxicity experiments with curcumin-loaded particles, an Alamar blue cell viability assay was performed to determine at what concentrations "free" curcumin was toxic to the cells. As shown in Figure 9a, curcumin was non-toxic to both MDA-MB-231 and MDA-MB-468 cells at concentrations up to ~26 μg/mL, while

higher concentrations resulted in toxicity. Based on these results, the same cell lines were incubated with **P2** and **P2-FA** at particle concentrations corresponding to curcumin concentrations in the range of 0.52 – 260 μg/mL. As shown in Figure 9b, the MDA-MB-231 cells were more resistant to curcumin. This was not surprising, as these cells are known to be highly aggressive and often resistant to different types of anti-cancer treatment.[67,68] It may also be related to the lower uptake of particles into these cells as shown in Figure 7b. The MDA-MB-468 cells exhibited less than 50% viability when exposed to **P2** and **P2-FA** at the highest concentrations. This toxicity can be attributed to their general susceptibility to treatment, as well as their increased uptake of the particles. The cell viabilities following treatment with the equivalent dose of curcumin in particles relative to the free drug were somewhat higher, which can likely be attributed to the gradual release of curcumin from these systems. While the slower release of drug can result in decreased toxicity in these *in vitro* assays, it is still a desirable feature of the system as it can afford protection of curcumin from metabolic degradation *in vivo*, allowing it to reach its target site at higher concentrations. At the highest concentration tested, MDA-MB-468 cells treated with **P2-FA-C** had slightly lower viability than those treated with **P2-C** but this difference was not statistically significant. It was demonstrated earlier that the drug loading content of **P2-FA-C** (9.0 ± 0.4 wt%) is only about one third that of **P2-C** (26 ± 2 wt%). This means that for **P2-FA-C** to deliver the equivalent dose into cells, more it must undergo almost 3-fold higher uptake relative to **P2-C**. Thus some potential relative enhancement in efficacy of **P2-FA-C** due to FA targeting versus **P2-C** may be unrealized in this *in vitro* study.

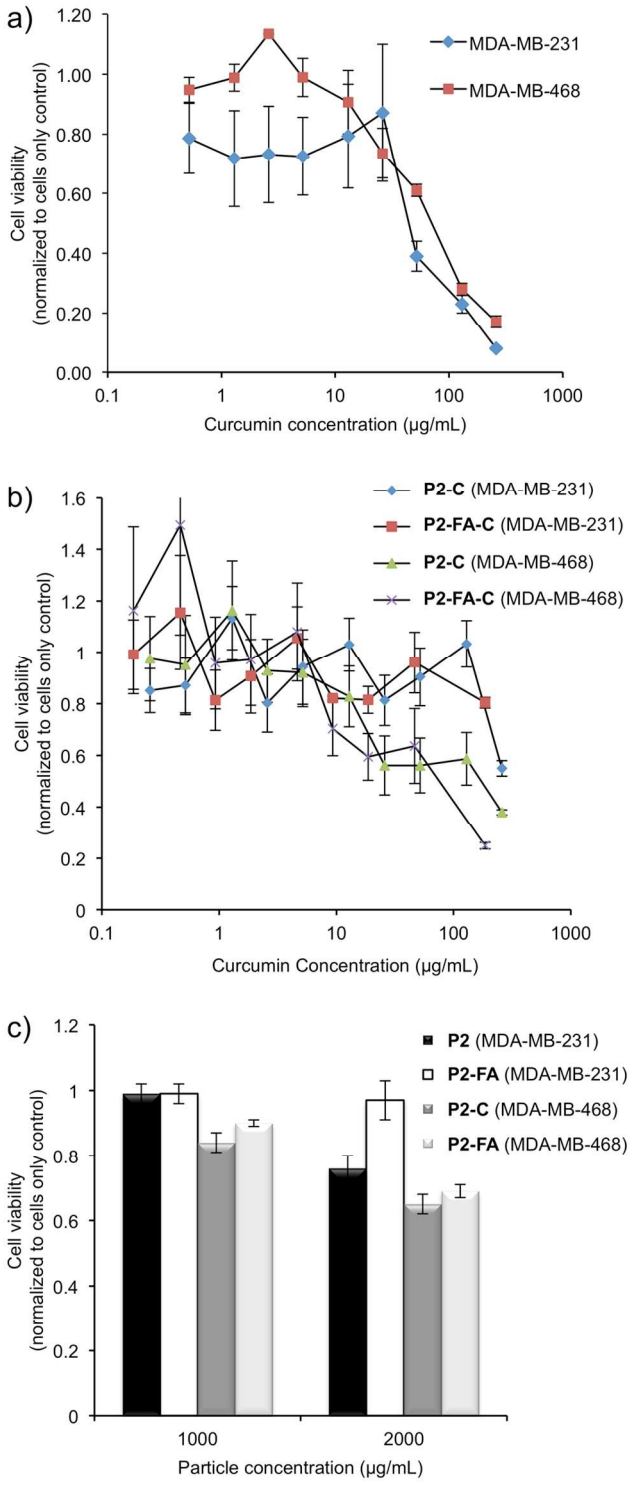

Figure 9. *In vitro* cytotoxicity of a) free curcumin; b) curcumin-containing particles **P2-C** and **P2-FA-C**; c) **P2** and **P2-FA** in MDA-MB-231 and MDA-MB-468 cells as

measured by the Alamar blue cell viability assay following 48 hour incubation with the samples.

To demonstrate that the toxicity indeed arose from curcumin rather than the particles themselves, the viabilities of MDA-MB-231 and MDA-MB-468 cells exposed to **P2** and **P2-FA** without curcumin were evaluated at the highest concentrations used in the above studies. As shown in Figure 9c, at 1000 μg/mL, neither **P2** nor **P2-FA** resulted in any toxicity to MDA-MB-231, and >80% cell viability was measured for MDA-MB-431 cells. At 2000 μg/mL, more cell death was observed for both cell lines, but interestingly the cell viability was still >90% for **P2-FA** in MDA-MB-231 cells. This suggests that FA in some way masks the toxicity of the particles. This might be explained by the fact that conjugation of FA to the PPG-NH_2 on the surfaces of the particles masks these cationic amines by converting them to amides. Cationic particles are suggested to impart toxicity through mechanisms such as membrane disruption.[69]

Conclusions

Magnetite was synthesized using a precipitation method in the presence of PPG-NH_2 and β-CD, resulting in the formation of PPG-NH_2 and β-CD-coated nanoparticles that assembled reversibly to form aggregates. The sizes of the aggregates depended on the concentrations and ratios of PPG-NH_2 and β-CD. The magnetite structure was not affected by the presence of the polymer coating and the magnetic coercivities of the particles were only modestly reduced by the presence of the coating. The terminal amine of PPG-NH_2 was used to conjugate FA as a targeting group using a dehydrative coupling method. The loading and release of curcumin into the β-CD cavities of both untargeted

and FA-functionalized particles was investigated. It was found that curcumin loadings were 23 - 26 wt% for the untargeted particles but 9 - 12 wt% for the FA-functionalized particles, presumably due to the occupation or blocking of the β-CD cavities by FA. Sustained release of curcumin over a period of a few days was achieved for **P2-C** and **P2-FA-C**. The *in vitro* properties of this new delivery system were also investigated. First, it was shown that relative to MDA-MB-231, MDA-MB-468 cells expressed elevated levels of the FA receptor. This translated into **P2-FA** exhibiting increased uptake into MDA-MB-468 cells relative to MDA-MB-231 cells and relative to **P2** into MDA-MB-468 cells, although the MDA-MB-468 cells generally displayed higher levels of particle uptake in comparison to MDA-MB-231. Particles **P2-FA** also exhibited increased uptake in MDA-MB-231 cells relative to **P2**. While susceptible to treatment with free curcumin, MDA-MB-231 cells were relatively resistant to treatment with **P2-C** and **P2-FA-C** at the concentrations tested and it was not possible to test higher concentrations due to the background toxicities of the curcumin-free particles. **P2-C** and **P2-FA-C** were toxic to MDA-MB-468 cells, although slightly less toxic than the equivalent dose of free drug, which can likely be attributed to the gradual release of curcumin from these vehicles. Finally, no significant differences in toxicity were observed for **P2-C** and **P2-FA-C**. Although, **P2-FA-C** exhibits increased cell uptake, it also has a ~3-fold lower curcumin loading, meaning that similar doses of curcumin are delivered to cells for **P2-C** and **P2-FA-C** under these static culture conditions. Still **P2-FA-C** is expected to provide increased selectivity for cancer cells *in vivo* potentially resulting in increased efficacy and fewer side effects. The curcumin loading can likely be improved through a reduction in the amount of conjugated FA and by increasing the content of β-CD on the particles.

Experimental section

General materials

$FeSO_4 \cdot 7H_2O$, NH_4OH and DMSO were purchased from VWR International. β-CD, PPG-NH_2 (2000 g/mol), curcumin, and DIPEA were purchased from Sigma-Aldrich. FA and FITC were purchased from Alfa Aesar. EDC was purchased from Advanced ChemTech. All growth media and supplements for the *in vitro* studies were obtained from Invitrogen (Carlsbad, CA). Fetal bovine serum (FBS) was obtained from Sigma-Aldrich (St. Louis, MO). All plastics were from Nunc™ (Thermo Fisher Scientific, Ottawa, ON).

Dynamic light scattering (DLS)

The Z-average aggregate diameter was determined using a Zetasizer Nano ZS instrument (Malvern Instruments). Samples were prepared at concentrations of 0.50 mg/mL and analyzed at a measurement angle of 173° at room temperature. Samples were run three times each in order to obtain a standard deviation value. The mean diameters of the individual particles and the polydispersity indices were determined using a Zetasizer 3000 HS_A (Malvern Instruments) at a scattering angle of 90° and room temperature. Nanoparticle suspensions (1.0 mg/mL) were prepared and diluted by a factor of 45 to obtain homogeneous suspensions of nanoparticles. Three runs were carried out per sample in order to obtain a standard deviation.

Transmission electron microscopy (TEM)

TEM imaging was performed using a Philips CM 10 transmission electron microscope operating at 80 kV. Samples were prepared on Formvar/carbon-coated-100-mesh copper grids. One drop of a 0.50 mg/mL particle suspension was used to cover the grid surface.

Excess water was removed using fine filter paper, and the grid was left for approximately 30 minutes to dry in air prior to imaging.

Fourier transform infrared (FTIR) spectroscopy

A Bruker-Tensor 27 spectrophotometer was used to obtain the FTIR spectra of the samples in the solid state. Samples were mixed with potassium bromide in a 1.0:10 w/w ratio and pressed into a disc prior to examination. Samples were scanned between 4000 – 600 cm^{-1} at a scanning speed of 4 cm^{-1}.

Vibrating sample magnetometry measurements

A model 74035 vibrating sample magnetometer (LakeShoreCryotronics Inc.) was used to explore the magnetic properties of the samples. Approximately 15 mg of sample were added in the sample holder, after which the sample was exposed to a magnetic field range of ±10000 G. Samples were studied at 25°C.

Preparation of particles P1 and representative particle preparation procedure.

Particles were synthesized based on a modification of the method reported by Ragab *et al*.[56] 1.40 g (5 mmol) of the $FeSO_4 \cdot 7H_2O$ were dissolved in 50 mL of distilled water. 0.50 mL (0.25 mmol) of PPG-NH_2 was added to the solution with stirring (400 rpm) and left until a color change from green to orange/yellow was observed (~ 10 minutes). 1.2 g (1.0 mmol) of β -CD dissolved in 20 mL of NH_4OH was gradually added to this mixture, at which point stirring was immediately increased to 1200 rpm and the temperature was increased to 80°C. The mixture was covered and stirred for 90 minutes. The particles were separated using a magnet and the supernatant was removed carefully using a pipette. The particles were then redispersed in distilled water. The sample was then recollected using the magnet and the distilled water was removed before the sample was redispersed

in ethanol. The sample was washed 3 times in ethanol using this procedure, and then dried at 60 °C. Particles **P2** – **P4** were prepared in the same manner, but the amounts of PPG-NH_2 and β-CD were adjusted according to Table 1.

Preparation of P1-FA and representative procedure for the conjugation of FA to particles.

Under a nitrogen atmosphere, 20 mg (46 μmol) of FA were dissolved in 10 mL of DMSO containing 20 μL (92 μmol) of DIPEA. This solution was added to 20 mg of particles **P1**, after which 10 mL of DMSO containing 7 mg (46μmol) of EDC were added under nitrogen. The samples were left shaking in a water bath for 3 hours at room temperature, and then at 35°C for 2 days. After removal of the samples from the water bath, the particles were left on a magnetic plate to settle. After separation using a magnet, the supernatant was removed, and the samples were redispersed in ethanol for washing. The samples were recollected with a magnet, the ethanol supernatant removed, and the samples were dispersed again in ethanol. This washing procedure was carried out 3 times, and the samples were dried at 50°C. The folic acid content in the combined supernatant was analyzed using UV-visible spectroscopy relative to a calibration curve ($\varepsilon = 29600\ M^{-1}cm^{-1}$) to quantify the amount of folic acid that has been conjugated to the particles.

Curcumin loading

Samples were loaded with curcumin via a modification to the method reported by Yallapu *et al.*[44] 10 mg of particles were dispersed in 2.8 mL of distilled water under stirring at 400 rpm. In the loading optimization study, curcumin (1.0, 1.5, 2.0, 3.0, or 5.0 mg) was dissolved in 200 μL of acetone and added dropwise to the particle suspension. Following the optimization experiment, 3.0 mg of curcumin was used in the preparation

of **P1-C**, **P2-C**, **P1-FA-C**, and **P2-FA-C**. The mixture was stirred for 24 hours at room temperature. The resulting curcumin-loaded particles were thoroughly washed with distilled water by magnetically collecting the samples, removing the liquid, and resuspending the particles in distilled water. The washing process was carried out 6 times. Samples were then freeze dried to obtain dry nanoaggregates. To determine the loading efficiency, 5.0 mg of curcumin-loaded particles were suspended in 10 mL of ethanol. The samples were left shaking in a water bath at 25 °C for 24 hours, after which samples were removed from the water bath and placed on a magnetic plate to allow the particles to settle. The liquid was collected using a pipette and the curcumin content was measured using UV-visible spectroscopy at 427 nm (ε = 50800 $M^{-1}cm^{-1}$ in ethanol).

Curcumin release

In vitro curcumin release was carried out at 37 °C in a water bath under constant shaking. 1.0 mg of curcumin-loaded particles was dispersed in 10 mL of phosphate buffered saline (PBS) containing 0.10 vol% Tween 80. At predetermined intervals, the particles were separated by the use of a magnet, and the liquid was collected and replaced by fresh buffer/Tween solution. The concentration of released curcumin in the liquid was measured by UV-visible spectroscopy based on the absorbance at 427 nm (ε = 53000 $M^{-1}cm^{-1}$ in PBS).

Preparation of fluorescein-labeled particles

1.0 mg of FITC was dissolved in 3 mL of acetone/water (0.3/2.7 v/v) and added to a dispersion of particles (10 mg) in 10 mL of PBS. The reaction was stirred at 1000 rpm in the dark for 24 hours at room temperature. The resulting FITC-labeled samples were washed with PBS and stored at 4 °C. The relative fluorescence of FITC-labeled **P2** and

P2-FA was measured by fluorescence spectroscopy. 1 mg of FITC-labeled particles was suspended in 1 mL of PBS and the fluorescence was measured over an emission range of 450 – 650 nm, using an excitation wavelength of 494 nm on a QM-4/2006 SE spectrofluorometer from Photon Technology International. The relative fluorescence of the samples were within ~10%, indicating that they could be compared effectively by flow cytometry in subsequent experiments.

Cell culture

MDA-MB-231 cells were obtained from American Type Culture Collection (Manassas, VA) and maintained in Dulbecco's Modified Eagle's Medium (DMEM/F12) containing 10% fetal bovine serum (FBS). MDA-MB-468 cells were obtained from Dr. Janet Price (MD Anderson Cancer Center, Houston, TX) and maintained in α-Minimal Essential Medium (MEM) containing 10% FBS. All cells were incubated at 37 °C under a 5% CO_2 atmosphere.

Flow cytometry analysis

For assessment of FA receptor expression, MDA-MB-231 and MDA-MB-468 human breast cancer cells were harvested and stained with a mouse anti-human folate receptor antibody (LK26, Abcam Inc, Cambridge MA) for 30 min at 4 °C. After removal of excess antibody by PBS washing, cells were incubated with AlexaFluor488-conjugated goat anti-mouse IgG (Life Technologies) for another 30 min at 4 °C, washed with PBS, and analyzed by flow cytometry using a Beckman Coulter EPICS XL-MCL flow cytometer.

For assessment of particle uptake, cells were seeded into 60 mm culture dishes and grown until 80% confluent. FITC-labeled **P2** or **P2-FA** (2000 μg/mL) were added to the cells.

After 4 hours incubation at 37 °C, particles that were not internalized were washed away using PBS and cells were harvested. Extracellular FITC was quenched by incubating with 200 μg/mL Trypan Blue (Sigma-Aldrich) for 10 min at room temperature. Cells were washed using PBS and analyzed by flow cytometry.

Fluorescence confocal microscopy

MDA-MB-231 and MDA-MB-468 human breast cancer cells were seeded onto 60 mm glass-bottom culture dishes and grown overnight. FITC-labeled **P2** or **P2-FA** (2000 μg/mL) were added to the cells. After 4 hours incubation at 37 °C, particles that were not internalized were washed away using PBS and extracellular fluorescein was quenched by incubating with 200 μg/ml Trypan Blue (Sigma-Aldrich) for 10 min at room temperature. Cells were washed using PBS, fixed by 2% paraformaldehyde, and imaged by confocal microscopy.

***In vitro* cytotoxicity assays**

MDA-MB-231 and MDA-MB-468 cells were plated in 100 μL of culture medium at a density of 2.5 x 10^4 cells/well in 96-well plates. After 24 hours, various treatments (**P2**, **P2-FA**, **P2-C**, **P2-FA-C**, or free curcumin were addedat varying concentrations to the cells and incubated for 48 hours. Cell viability was determined using the Alamar Blue Assay (Life Technologies, Inc., Burlington, ON).

Acknowledgements

We thank the Natural Sciences and Engineering Research Council of Canada Discovery Grant Program, the Canada Research Chairs program, and the Ontario Graduate

Scholarships program for funding this work. Olivier Nguon is thanked for assistance with acquiring the TEM images.

References

1 Z. Amoozgar and Y. Yeo, *Wiley Interdiscip. Rev. Nanomed. Nanobiotechnol.*, 2012, **4**, 219.

2 J. Buse and A. El-Aneed, *Nanomedicine*, 2010, **5**, 1237.

3 A. Kumari, S. K. Yadav and S. C. Yadav, *Colloids Surf., B*, 2010, **75**, 1.

4 A. K. Agnihotri, O. I. Aruoma and T. Bahorun, *Arch. Med. Biomed. Res.*, 2014, **1**, 1.

5 P. Singh and A. Singh, *J. Cancer Ther. Res.*, 2012, DOI : http://dx.doi.org/10.7243/2049-7962-1-5.

6 R. Guo and X. Shi, *Curr. Drug Metab.*, 2012, **13**, 1097.

7 M. Stanczyk, A. Dziki and Z. Morawiec, *Curr. Med. Chem.*, 2012, **19**, 4896.

8 C. Deng, Y. Jiang, R. Cheng, F. Meng and Z. Zhong, *Nano Today*, 2012, **7**, 467.

9 N. Nishiyama, H. Cabral and K. Kataoka in *Drug Delivery in Oncology*, eds. F. Kratz, P. Senter, H. Steinhagen, Wiley-VCH Verlag GmbH & Co. KGaA, Weinheim, 2011, pp. 1051-1069.

10 W. T. Al-Jamal and K. Kostarelos, *Acc. Chem. Res.*, 2011, **44**, 1094.

11 F. Meng, R. Cheng, C. Deng and Z. Zhong in *Functional Polymers for Nanomedicine*, ed. Y. Shen, The Royal Society of Chemistry, Cambridge, 2013, pp. 144-157.

12 E. Brewer, J. Coleman and A. Lowman, *J. Nanomater.*, 2011, **2011**, Article ID 408675.

13 U. Prabhakar, H. Maeda, R. K. Jain, E. M. Sevick-Muraca, W. Zamboni, O. C. Farokhzad, S. T. Barry, A. Gabizon, P. Grodzinski and D. C. Blakey, *Cancer Res.*, 2013, **73**, 2412.

14 F. Danhier, O. Feron and V. Preat, *J. Controlled Release*, 2010, **148**, 135.

15 L. Brannon-Peppas and J. O. Blanchette, *Adv. Drug Delivery Rev.*, 2004, **56**, 1649.

16 J. C. Kraft, J. P. Freeling, Z. Wang and R. J. Y. Ho, *J. Pharm. Sci.*, 2014, **103**, 29.

17 S. Svenson, *Wiley Interdiscip. Rev. Nanomed. Nanobiotechnol.*, 2014, **6**, 125.

18 S. Laurent, A. A. Saei, S. Behzadi, A. Panahifar and M. Mahmoudi, *Exp. Opin. Drug Deliv.*, 2014, **11**, 1449.

19 Y.-X. J. Wang, S. Xuan, M. Port and J.-M. Idee, *Curr. Pharm. Des.*, 2013, **19**, 6575.

20 J. Gautier, E. Allard-Vannier, E. Munnier, M. Souce and I. Chourpa, *J. Controlled Release*, 2013, **169**, 48.

21 F. Liu, S. Laurent, H. Fattahi, L. V. Elst and R. N. Muller, *Nanomedicine*, 2011, **6**, 519.

22 S. Laurent, L. V. Elst and R. N. Muller in *The Chemistry of Contrast Agents in Medical Magnetic Resonance Imaging*, eds. A. S. Merbach, L. Helm, E. Toth, John Wiley & Sons, Ltd., Hoboken, 2013, pp. 427-447.

23 V. Mody Vicky, A. Singh and B. Wesley, *Eur. J. Nanomed.*, 2013, **5**, 11.

24 K. Turcheniuk, A. V. Tarasevych, V. P. Kukhar, R. Boukherroub and S. Szunerits, *Nanoscale*, 2013, **5**, 10729.

25 J. Gautier, E. Allard-Vannier, K. Herve-Aubert, M. Souce and I. Chourpa, *Nanotechnology*, 2013, **24**, 432002.

26 L. Zhang, Y. Li and J. C. Yu, *J. Mater. Chem. B*, 2014, **2**, 452.

27 H. Hatcher, R. Planalp, J. Cho, F. M. Torti and S. V. Torti, *Cell Mol. Life Sci.*, 2008, **65**, 1631.

28 M. Salem, S. Rohani and E. R. Gillies, *RSC Adv.*, 2014, **4**, 10815.

29 A. Shehzad and Y. S. Lee, *Biofactors*, 2013, **39**, 27.

30 S. C. Gupta, S. Prasad, J. H. Kim, S. Patchva, L. J. Webb, I. K. Priyadarsini and B. B. Aggarwal, *Nat. Prod. Rep.*, 2011, **28**, 1937.

31 Y. Gao, Z. Li, M. Sun, C. Guo, A. Yu, Y. Xi, J. Cui, H. Lou and G. Zhai, *Drug Deliv.*, 2011, **18**, 131.

32 N. R. Goud, K. Suresh, P. Sanphui and A. Nangia, *Int. J. Pharm.*, 2012, **439**, 63.

33 P. Sanphui, N. R. Goud, U. B. R. Khandavilli and A. Nangia, *Cryst. Growth Des.*, 2011, **11**, 4135.

34 L. Li, F. S. Braiteh and R. Kurzrock, *Cancer*, 2005, **104**, 1322.

35 N. Saengkrit, S. Saesoo, W. Srinuanchai, S. Phunpee and U. R. Ruktanonchai, *Colloids Surf., B*, 2014, **114**, 349.

36 D. Sun, X. Zhuang, X. Xiang, Y. Liu, S. Zhang, C. Liu, S. Barnes, W. Grizzle, D. Miller and H. G. Zhang, *Mol. Ther.*, 2010, **18**, 1606.

37 C. Mohanty, S. Acharya, A. K. Mohanty, F. Dilnawaz and S. K. Sahoo, *Nanomedicine*, 2010, **5**, 433.

38 S. Podaralla, R. Averineni, M. Alqahtani and O. Perumal, *Mol. Pharm.*, 2012, **9**, 2778.

39 X. Gao, F. Zheng, G. Guo, X. Liu, R. Fan, Z.-Y. Qian, N. Huang and Y.-Q. Wei, *J. Mater. Chem. B*, 2013, **1**, 5778.

40 H. Sasaki, Y. Sunagawa, K. Takahashi, A. Imaizumi, H. Fukuda, T. Hashimoto, H. Wada, Y. Katanasaka, H. Kakeya, M. Fujita, K. Hasegawa and T. Morimoto, *Biol. Pharm. Bull.*, 2011, **34**, 660.

41 R. Misra and S. K. Sahoo, *Mol. Pharm.*, 2011, **8**, 852.

42 K. Sindhu, A. Rajaram, K. J. Sreeram and R. Rajaram, *RSC Adv.*, 2014, **4**, 1.

43 M. M. Yallapu, M. Jaggi and S. C. Chauhan, *Colloids Surf., B*, 2010, **79**, 113.

44 M. M. Yallapu, S. F. Othman, E. T. Curtis, N. A. Bauer, N. Chauhan, D. Kumar, M. Jaggi and S. C. Chauhan, *Int. J. Nanomedicine*, 2012, **7**, 1761.

45 M. M. Yallapu, S. F. Othman, E. T. Curtis, B. K. Gupta, M. Jaggi and S. C. Chauhan, *Biomaterials*, 2011, **32**, 1890.

46 V. Yadav, S. Suresh, K. Devi and S. Yadav, *AAPS PharmSciTech*, 2009, **10**, 752.

47 H. H. Tønnesen, M. Másson and T. Loftsson, *Int. J. Pharm.*, 2002, **244**, 127.

48 A. Harada, M. Okada, J. Li and M. Kamachi, *Macromolecules*, 1995, **28**, 8406.

49 Y. Liu, Y.-W. Yang, Y. Chen and H.-X. Zou, *Macromolecules*, 2005, **38**, 5838.

50 Y. Lu and P. S. Low, *J. Controlled Release*, 2003, **91**, 17.

51 N. Parker, M. J. Turk, E. Westrick, J. D. Lewis, P. S. Low and C. P. Leamon, *Anal. Biochem.*, 2005, **338**, 284.

52 K. Yan, P. Li, H. Zhu, Y. Zhou, J. Ding, J. Shen, Z. Li, Z. Xu and P. K. Chu, *RSC Adv.*, 2013, **3**, 10598.

53 S. F. Hasany, I. Ahmed, J. Rajan and A. Rehman, *Nanosci. Nanotechnol.*, 2012, **2**, 148.

54 D. Gu and F. Schuth, *Chem. Soc. Rev.*, 2014, **43**, 313.

55 L. Zhang, W.-F. Dong and H.-B. Sun, *Nanoscale*, 2013, **5**, 7664.

56 D. M. Ragab, S. Rohani and S. Consta, *Int. J. Nanomedicine*, 2012, **7**, 3167.

57 E. R. Leite and C. Ribeiro *Crystallization and Growth of Colloidal Nanocrystals*, Springer, New York, 2011.

58 G. F. Goya, T. S. Berquo, F. C. Fonseca and M. P. Morales, *J. Appl. Phys.*, 2003, **94**, 3520.

59 X. Zhao, H. Zhao, Z. Chen and M. Lan, *J. Nanosci. Nanotechnol.*, 2014, **14**, 210.

60 B. Stuyven, Q. Chen, W. Van de Moortel, H. Lipkens, B. Caerts, A. Aerts, L. Giebeler, B. V. Eerdenbrugh, P. Augustijns, G. Van de Mooter, J. V. Humbeeck, J. Vanacken, V. V. Moshchalkov, J. Vermant and J. A. Martens, *Chem. Commun.*, 2008, 49.

61 R. M. Cornell and U. Schwertmann, *The Iron Oxides*, Wiley-VCH Verlag GmbH & Co. KGaA, Weinheim, 2004.

62 J. Lee, S. Zhang and S. Sun, *Chem. Mater.*, 2013, **25**, 1293.

63 N. Lee and T. Hyeon, *Chem. Soc. Rev.*, 2012, **41**, 2575.

64 W. Cai and J. Wan, *J. Colloid Interface Sci.*, 2007, **305**, 366.

65 M. S. Jhaveri, A. S. Rait, K.-N. Chung, J. B. Trepel and E. H. Chang, *Mol. Cancer Ther.*, 2004, **3**, 1505.

66 V. Mamaeva, J. M. Rosenholm, L. T. Bate-Eya, L. Bergman, E. Peuhu, A. Duchanoy, L. E. Fortelius, S. Landor, D. M. Toivola, M. Linden and C. Sahlgren, *Mol. Ther.*, 2011, **19**, 1538.

67 H. Rochefort, M. Glondu, M. E. Sahla, N. Platet and M. Garcia, *Endocr. Relat. Cancer*, 2003, **10**, 261.

68 J. Chen, L. Lu, Y. Feng, H. Wang, L. Dai, Y. Li and P. Zhang, *Cancer Lett.*, 2011, **300**, 48.

69 P. R. Leroueil, S. A. Berry, K. Duthie, G. Han, V. M. Rotello, D. Q. McNerny, J. R. Baker, B. G. Orr and M. M. Banaszak Holl, *Nano Lett.*, 2008, **8**, 420.